Catalysis Today 141 (2009) 168–175

Contents lists available at ScienceDirect

Catalysis Today

journal homepage: www.elsevier.com/locate/cattod

NiMo supported acidic catalysts for heavy oil hydroprocessing☆

Carolina Leyva [a], Mohan S. Rana [a,*], Fernando Trejo [b], Jorge Ancheyta [a]

[a] Instituto Mexicano del Petróleo, Eje Central Lázaro Cárdenas Norte 152, Col. San Bartolo Atepehuacan, México D.F. 07730, Mexico
[b] Centro de Investigación en Ciencia Aplicada y Technologia Avanzada, Unidad Legaria, Instituto Politécnico Nacional (CICATA-IPN), Legaria 694, Col. Irrigación, México D.F. 11500, Mexico

ARTICLE INFO

Article history:
Available online 20 May 2008

Keywords:
NiW/SiO_2-Al_2O_3
Acidic support
SEM–EDX
Cumene cracking
HDS
Hydrodemetallization
Heavy crude oil

ABSTRACT

Large pore diameter Al_2O_3-SiO_2 acidic mixed oxide supports were prepared by using homogeneous co-precipitation method. The acidic properties of supports (oxide) and supported catalysts (sulfided) were chemically probed with cumene cracking (HCR) into propane and benzene at atmospheric pressure and 400 °C. NiMo supported hydroprocessing catalysts activities were also evaluated with heavy Maya crude oil. The use of acidic support is to optimize yield of high octane gasoline components, *i.e.* selective cracking of complex crude oil molecule. The supported fresh and spent catalysts were characterized by means of N_2 adsorption–desorption and SEM–EDX spectroscopic techniques. The results point out that deactivation takes place mainly at the entrance of pore due to coke deposition, while the depositions of vanadium and nickel sulfides mainly depend on the diameter of the pores. The results also indicated that the deactivation due to carbon deposition is carried out at initial hours of the crude oil processing. The large pore diameter catalyst contains higher amounts of deposited species, which are distributed proportionally along the extrudate radius, while for smaller pore diameter catalyst the deposition mainly occurs on the extrudate surface.

1. Introduction

The petroleum industry is increasingly concerned about heavy and extra-heavy oil processing. These crudes are also being considered as a future option for fuel production using different processes. In general crude oils are composed by virtually infinite number of different complex hydrocarbons containing large amounts of sulfur, nitrogen and metals. On the contrary, the increasing demand for middle distillate fuels with improved quality, which have limited reserves in the nature, has been requested by the market due to stricter environmental legislations. To achieve such specifications refiners need to look for improved or new catalysts technologies, which must be able to satisfy the middle distillate yield as well as remove inorganic contaminants (S, N, Ni, V, Fe, Ca, etc.) from the heavy crude oil. However, the direct hydroprocessing of virgin heavy crude oil will not produce commercial fuels rather it is a primary process to reduce metals and asphaltene content in heavy oil, which will be effectively used as FCC and hydrocracking feedstock or for synthetic crude oil production [1].

Mixed oxides have some acid sites which demonstrated to possess notable activity for hydrodemetallization (HDM) and cracking reactions. [2,3]. Also in order to improve both hydrodesulfurization (HDS) and hydrogenation activity, nickel is included in the catalyst formulation. On the other hand, the relative contributions of the catalytic reaction and thermal cracking on the hydrocracking of heavy oil have been evaluated in detail and it is reported that asphaltenes conversion into light oil fractions is mainly due to thermal cracking [4] and the main role of the catalyst is to supply hydrogen to the cracked fraction and prevent its carbonization. Moreover, catalyst deactivation can be partially avoided by using high hydrogen pressure, in which multifaceted heterolytic dissociative role of hydrogen is expected during the hydroprocessing of heavy oil (i) to regenerate Brønsted acid sites, ability to break C–C bonds and produce carbocations; (ii) to terminate radicals formed by C–C bond breaking; and (iii) to hydrogenate C=C bond and decrease carbonaceous material, but the investment of the process increases proportionally, thus, increasing the hydrogen pressure is not a solution.

The hydroprocessing of heavy oils is a complex task due to the presence of high contaminants content, particularly metals (Ni and V) and conradson carbon, which cause poisoning and rapid deactivation of the catalysts commonly used for hydroprocessing. Asphaltene is the most difficult molecule to be processed in the

☆ This forms part of the plenary lecture delivered in the symposium.
* Corresponding author. Tel.: +52 55 9175 8418; fax: +52 55 9175 8429.
E-mail addresses: msingh@imp.mx, mohan.rana@gmail.com (M.S. Rana).

0920-5861/$ – see front matter © 2008 Elsevier B.V. All rights reserved.
doi:10.1016/j.cattod.2008.03.030

heavy crude oil than any other molecule because most of the metals, sulfur and nitrogen atoms are associated with the asphaltene molecule. Therefore, to remove the metals (Ni or V) and sulfur from the heavy oil it is mandatory to breakdown the molecule of asphaltene. On the other hand, during deactivation of catalyst particularly asphaltenes quality rather than quantity plays a more important role [5]. An increase in asphaltene aromaticity and its ring condensation brings higher coke deposition, thus, sub-fraction of asphaltenes may provide different concentration of carbon deposition on the catalyst [6,7]. As an affect of asphaltene nature polar fractions show a high propensity to adsorb onto the catalyst surface [8].

The purpose of this work is to develop a catalyst with significant acidic sites and large pore, at moderate hydrogen partial pressure operation, which helps in hydrodemetallization and effective diffusion of complex molecules into the pores. Particularly, amorphous Al_2O_3-SiO_2 based NiMo catalysts, which possess weaker acidity than zeolites, were studied with different SiO_2 contents in support in order to vary the acidity and their effect on HDM activity. The nature of SiO_2-Al_2O_3 support, predominatly to its acidity, influences the electron deficiency of active metals species which are deposited on the support. The study leads to an important contribution in development of a catalyst which would be able to have more metal deposition and higher cracking function due to the support contribution.

2. Experimental

High specific surface area and large pore diameter SiO_2-Al_2O_3 supports were prepared by homogeneous co-precipitation method using appropriate amount of sodium silicate (Na_2SiO_3), aluminium nitrate, and NH_4OH as precipitating agent with continuous stirring. At the initial stage sodium silicate gel was prepared at low pH at around 3.5, once the silica gel was obtained the aluminium nitrate was precipitated at pH 9.5. The mixed sol–gel material was aged at 60 °C for 12–15 h, and subsequently filtered with de-ionized water. After complete removal of sodium ions by washing, the precipitate was dried overnight at 120 °C and calcined at 550 °C for 5 h. The different compositions of Al_2O_3-SiO_2 (AS) mixed oxides were prepared and these support compositions are hereafter designated as AS-31, AS-56, and AS-78, where the number indicated the molar ratio of Si/(Si + Al) = 0.31, 0.56, 0.78, respectively.

The NiMo catalysts were prepared by the incipient wetness co-impregnation (pH 5.5) method. An appropriate amount of ammonium heptamolybdate (AHM) (Fluka AR grade) and nickel nitrate was used in aqueous solution. The nickel promoted catalysts were dried in the presence of air at 120 °C overnight and calcined at 450 °C for 4 h. The compositions of support and supported catalysts are reported in Tables 1 and 2 respectively.

The surface morphology of catalysts was studied by means of elemental analysis with the SEM-FIB analytical instrument xT Nova NanoLab 200, combined with a dual high resolution focused ion beam using detector type SUTW, Sapphire with LEAP + crystals for the best light element performance of the Si(Li) detector. The sample was deposited on a carbon holder and evacuated at high vacuum (10^{-5} Torr) before images were taken. Five representative analyses were taken to confirm the results. The analysis was made across the radial line of the extrudate; points were chosen *e.g.* external, semi-external, center, and vice-versa.

The BET specific surface area (SSA), pore volume (PV) and pore size distribution (PSD) were carried out in a Quantochrome Nova 4000 equipment. Nitrogen gas was employed for SSA measurements at liquid nitrogen temperature (−196 °C). Prior to the adsorption, the samples were degassed for 3 h at 300 °C.

To evaluate the catalytic behavior with industrial feedstock the catalysts were tested in a high pressure micro up-flow reactor. The properties of the feedstock are presented in Table 3. The catalyst pretreatment and the hydrotreating reactions were carried out in the high pressure integral fixed-bed reactor. The reactor was loaded with oxidic catalyst with 3–5 mm extrudate size diluted with equal volume of SiC. The catalyst was sulfided *in-situ* using a mixture of dimethyldisulfide (DMDS), straight run gas oil (SRGO) and H_2. After depressurizing the reactor to atmospheric pressure, the sulfiding feed (1 wt.% DMDS + SRGO) containing ≈2.0 wt.% "S" was started to wet the catalyst bed at room temperature. The liquid was drained after 4 h, and then the temperature was linearly increased from 30 to 120 °C (30 °C/h) and kept at this value for 2 h. Later, the temperature was increased at the rate of 30 °C/h until 150 °C, at 2.8 MPa pressure and stayed 2 h, further increase of

Table 1
Support composition estimated by using SEM–EDX

Support name	Composition (wt.%)		
	Al_2O_3	SiO_2	Na_2O^*
AS-31	68.6	31.4	–
AS-56	43.6	55.6	0.8 (0.93)
AS-78	21.9	76.7	1.4 (1.54)

* The values in parentheses are obtained by the atomic absorption analysis.

Table 2
Composition and physical properties of catalysts

Catalysts properties		
	NiMo/AS-31	NiMo/AS-56
Catalyst composition (wt.%)		
MoO_3 (Mo)	6.9 (4.6)	6.9 (4.6)
NiO (Ni)	2.3 (1.7)	2.3 (1.7)
Catalyst physical properties		
Shape	Cylindrical extrudate	Cylindrical extrudate
Size (in.)	1/12	1/12
Specific surface area ($m^2\ g^{-1}$)	255.4	167.5
Average pore diameter (nm)	8.5	14
Total pore volume ($mL\ g^{-1}$)	0.54	0.59
% Micro-pore ($d < 2$ nm) vol. ($mL\ g^{-1}$)	1.2	1.4
% Meso-pore ($2 \geq d \leq 50$ nm) vol. ($mL\ g^{-1}$)	93.5	73.9
% Macro-pore ($d > 50$ nm) vol. ($mL\ g^{-1}$)	5.3	24.7

Table 3
Properties of the heavy hydrocarbon oil feed

Properties	Feedstock (Maya crude)
Elemental analysis (wt.%)	
C	86.9
H	5.3
N	0.3
S	3.52
Metal (wppm)	
Ni	49.5
V	273.0
Ni + V	322.5
Ca	11.26
Mg	2.04
Na	44.83
K	20.25
Fe	2.16
Asphaltene, wt.% (n-C_7 insol.)	12.7
Physical properties	
Density (20/4 °C)	0.9251
Pour point (°C)	−30
Ramsbottom carbon (wt.%)	10.87
API gravity	21.31

Table 4
Reaction conditions for fixed-bed integral reactors

Conditions	
Temperature (°C)	380
Pressure (MPa)	7.0
Hydrogen flow (L/h)	4.6
Flow of Maya crude (mL/h)	10
LHSV (h^{-1})	1.0
H_2 (std)/HC (m^3/m^3)	890.44
Mode of operation	Up-flow
Time-on-stream (h)	204
Catalyst volume, mL (g)	10 (6.8)
Extrudate diameter (mm)	2.2
Extrudate length (mm)	5–7
Feed composition tested	Pure Maya crude

temperature at 260 °C and dwelled for 3 h. The final temperature of sulfidation was 320 °C, which was stabilized for 5 h at 2.8 MPa. A detailed account of stepwise sulfidation is given elsewhere [9]. After sulfidation, the flow was switched to the Maya crude oil feed and the operating conditions were adjusted as shown in Table 4. The process conditions used are the typical ones for heavy crude oil processing of moderate severity of reactions. These conditions were selected based on the literature as well as on our own working experience with the Maya crude [10–12].

Metals (Ni, V) were analyzed in the feed and products using flame atomic adsorption spectrometry (ASTM D 5863-00a method). The total S content was analyzed with a HORIBA model SLFA-2100/2800 using scattered spectroscopy by sulfur generating fluorescent energy dispersive X-ray fluorescence. The X-ray beam was separated selectively with the help of a filter and detected as sulfur concentration. Nitrogen was measured by oxidative combustion and chemiluminescence (ASTM D 4629-02 method) at high temperature combustion in an oxygen rich atmosphere. Asphaltene is defined as the insoluble fraction in *n*-heptane, which is an indirect measure of dry-sludge formation.

3. Results and discussion

3.1. Synthesis of support

The catalysts supports were prepared by homogeneous precipitation method; the silica mixed sol–gel was converted into the sol by aging at 60 °C for 12 h. Fig. 1 is a flow diagram for aqueous precipitation of alumina–silica homogeneous sol–gel, starting from a solution of sodium silicate and then aluminium nitrate controlling the required pH with ammonium hydroxide. The syntheses of sol (dense particle) depend on the particle aggregation (1–5 nm in diameter) which is controlled by the aging time, temperature and pH of the silica–alumina co-gelled. During the aging period it is likely that the smaller particle will change into larger crystals particularly at pH higher than 7. An increase in particle expansion is known as *Ostwald ripening*, which augments the average particle diameter of the silica in the range of 5–10 nm, while at lower pH the particles swelling occurs only by 2–4 nm [13]. A silica and alumina gel is rapidly made, probably by polymerization to form siloxane type groups in the presence of ammonium hydroxide. This co-gel is then digested by partially hydrolyzed slowly aluminium species which break the Si–O–Si bonds and link to the gel by Si–O–Al kind of bonds or free silica and alumina atoms hydro-oxides particularly at enhanced digesting temperature. Moreover, the number of pores and the pore size distribution on micro-structure evolution are increased with the increase of densification rate, and the grain growth rate, while narrowing the pore size distribution has been predicted to inhibit

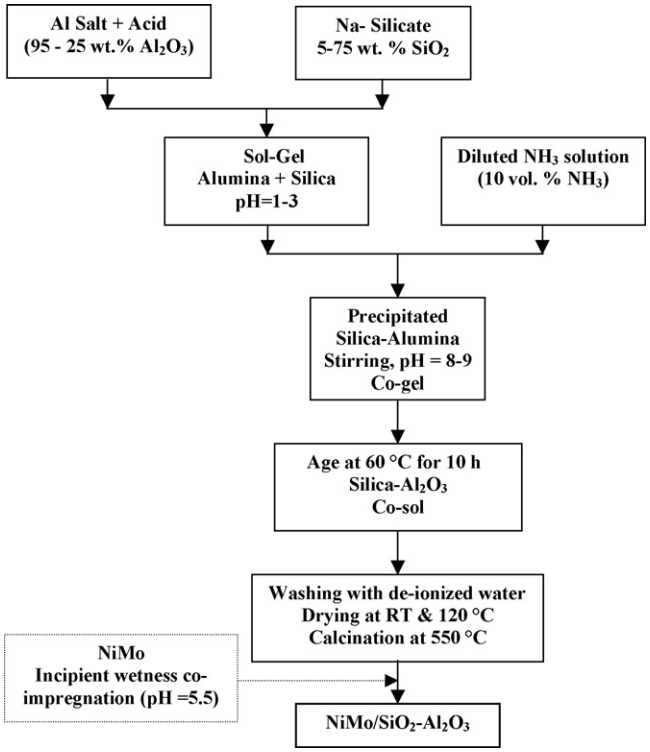

Fig. 1. Synthesis of SiO_2-Al_2O_3 NiMo supported catalysts.

grain growth indirectly [14]. Thus, the effects of processing conditions on the formation of alumina and silica sols from the hydrolysis of alkoxide precursors have been investigated at 20 °C, which are greatly formed form those processed at 95 °C. At low temperature processed sols, the aluminium is predominantly in the form of the poly-oxycation species while high temperature (95 °C) results in the growth of tetrahedral and octahedral alumina species [15].

3.2. Characterization

The composition of silica–alumina was determined by the scanning electron microscopy of the energy dispersive X-ray (SEM–EDX) point as well as linear analysis of the extrudate. The SEM–EDX provided physical and chemical characterization of solid materials, which indicated that the distribution of silica is homogeneous and the SEM images visibly found the presence of macro-pores probably linked in three dimensions. The composition of supports is reported in Table 1. Small amount of sodium content remained in the high silica samples, which may act as impurity in the catalysts.

The properties of the supports and catalyst in terms of composition and textural characterization are reported in Table 2. Mixed oxides have generally higher surface areas as compared with the pure alumina or silica oxides. The textural properties result indicates that the composition of support is the principal feature that ascertains the meso- and macro-pore structure of the mixed oxide and, consequently, allows control of the support characteristics. The typical N_2 adsorption isotherms of the calcined mixed oxides supported catalyst shows corresponding pore size distribution (PSD) profiles *type* IV and *type* II respectively for AS-31 and AS-56 derived from the BJH method. Both catalysts possess meso- as well as macro-pores, the corresponding BJH adsorption results of the pore structure are summarized in Table 2. The hysteresis curves of the adsorption–desorption isotherms of the two catalysts are quite different: *e.g.* in

the case of AS-56, the hysteresis loop is not very broad ($0.8 < P/P_0 < 0.9$), which confirmed the macro-pore structure with mono-modal pore distribution and low specific area, while the hysteresis loop of AS-31 is quite extended, which is typical of a catalyst of greater specific area and smaller pores. Concerning the pore size distribution of these materials from the results, it can be appreciated that the specific surface area in AS-56 is about 1.5 times smaller than that of AS-31. The variation in textural properties is due to the nature of alumina–silica and their particle size, which are different at each SiO_2/Al_2O_3 ratio reported in Table 2. In Table 2 the comparison was made between the AS-31 and AS-56 NiMo supported catalysts, since they have notable differences of textural properties. These results are in agreement with previously reported pore distribution measurements, all the supports contain meso-pores. The alumina rich samples have pore size between 1 and 10 nm, whereas the silica rich ones have pores of sizes between 10 and 30 nm [16].

The Al_2O_3-SiO_2 supported catalysts were characterized by using X-ray diffractograms to qualitatively determine the presence of crystalline silica and/or alumina phases after calcination [17]. The diffractograms are dominated at lower SiO_2 with the γ-Al_2O_3 phases, while increasing silica content the amorphous nature of solid is more evident due to the contribution of silica. The powder XRD diffractograms of the support and NiMo supported catalysts showed amorphous patterns with different SiO_2/Al_2O_3 ratios in the as-synthesized form, which indicated that the particle size is less than 4 nm, respectively, for support as well as supported phases. Generally, due to the low iso-electric point (IEP) of silica lower dispersion is expected, but in this study it did not happen since the metal loading is very low and the co-impregnation of NiMo was carried out relatively at lower pH (*i.e.* 5.5), which is at around the theoretical IEP of SiO_2-Al_2O_3 mixed oxide. However, the IEP will vary with the composition of Si/Al ratio. Nevertheless, we consider that the IEP of support will not differ in large scale, moreover, it is also reported that the sol–gel prepared silica presented rather high point of zero charge as reported in the literature [16].

3.3. Cumene hydrocracking (HCR)

The acidity of support increases with SiO_2 content up to 56 wt.% after that it decreases probably due to a reduction in Al–O–Si connectivity and as a result the number of Brønsted acid sites diminished [18]. The source of acidity in alumina–silica is due to the presence of Si^{4+} and Al^{3+} in tetrahedral environment of shared oxide ions. The net charge of ions (−eV) must be stabilized nearby positive ions such as protons (Brønsted acid sites). Thus, these Brønsted acidic sites can be converted into Lewis acid sites by heating. The deposition of molybdenum on SiO_2-Al_2O_3 supports leads to formation of surface Brønsted acid sites. The number of the Brønsted and Lewis acid sites in supported-molybdenum catalysts also depends on both the SiO_2 content and the type of support. Reaction rate of cumene hydrocracking for NiMo supported catalysts as function of SiO_2 content in the support is shown in Fig. 2. A significant acidity reduction is observed after NiMo incorporation on support and after sulfidation. However, in these catalysts (*i.e.* sulfided) the contribution of sulfhydryle (–SH) groups is also included [19–21]. Muralidhar et al. [22] studied the isooctene cracking over sulfided CoMo supported on silica and $CoMo/Al_2O_3$ catalysts modified by various additives and concluded that cracking function wielded due to the CoMo sulfide phase. While Sivasanker et al. [23] reported that the Mo supported Al_2O_3 catalyst created acid sites during sulfidation which are stronger than those of the support. Thus, the cracking activity is a contribution of both the support and supported acid sites phases.

The comparison of supports and catalysts indicates that the number of –OH group in mixed oxide support and its interaction

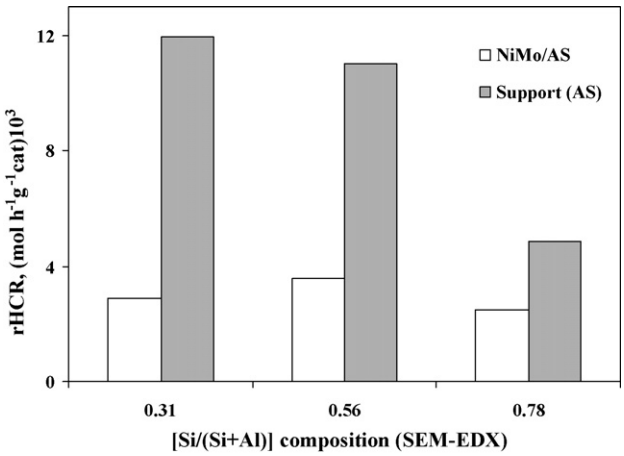

Fig. 2. Effect of silica content on the acidity of the support and supported catalysts.

with molybdenum and nickel provokes a decrease in Brønsted acidity. The acid sites, consisting of a sulfur vacancy on a molybdenum, nickel atom, or Brønsted acid sites; constituted of H atoms on the sulfur atoms (*i.e.* protons of SH^- groups). The ratio of support acidity/sulfided catalyst acidity increases up to 31 wt.% silica (*i.e.* 4.1, determined as the ratio of reaction rates of support and catalyst) and remains constant up to 56 wt.%, which decreases rapidly with further increase in silica content in the support. These results are indicating that the optimum dispersion of –SH groups is obtained along with support contribution at 56 wt.% silica and further increase in silica may decrease the interaction between the support and molybdenum. A decrease in support metal interaction occurs due to the excess of silica on support surface that encourages the formation of larger crystals of MoS_2. The similar tendency of acidity variation for both cases (support as well as supported catalyst) confirmed the contribution of support as well as supported phases. However, the supported catalyst showed higher acidity at 56/44 wt.% compared with the support whose maximum acidity is at 31 wt.% of silica in alumina. The aim of these cracking activities results is to find out a balance between acidity and textural properties of the sulfided catalysts, which is responsible for the cracking activity of heavy oil molecules, simultaneously, these acid sites are likely to be deactivated at faster rate by carbon deposition.

4. Maya heavy crude oil hydroprocessing

Two of the mixed oxide supported catalysts (NiMo/AS-0.31 and NiMo/AS-0.56) were tested for Maya heavy crude oil hydroprocessing. Both catalysts contain almost similar amount of Mo (4.6 wt.%) and Ni (1.74 wt.%), therefore, the number of catalytic sites is expected to be the same for both catalysts. The hydrodesulfurization results for both catalysts are reported in Fig. 3. The catalysts exhibited different behavior with time-on-stream particularly deactivation. The catalyst containing lower silica content (31 wt.%) and smaller pore diameter is having much better HDS activity and represents normal deactivation with time-on-stream [24–26]. However, the large pore diameter and high silica supported catalyst showed high initial activity but with time the catalyst deactivated at very fast rate. The HDS activity ratios (NiMo-AS-31/NiMo-AS-56) vary with time from 1.2 to 4.5 for initial and final activity, respectively. The deactivation behavior can be attributed to the presence of higher number of cracking sites as shown in Fig. 3, It is also expected that high silica supported catalyst has lower activity due to the low dispersion of catalytic sites, which is rather normal to aggregate molybdenum crystal in the case of high

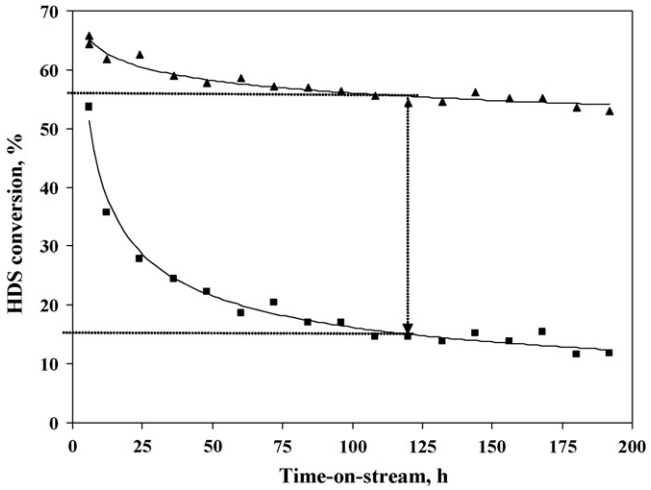

Fig. 3. Effect of support composition on the hydrodesulfurization of Maya heavy crude: [(▲) NiMo/AS-31; (■) NiMo/AS-56].

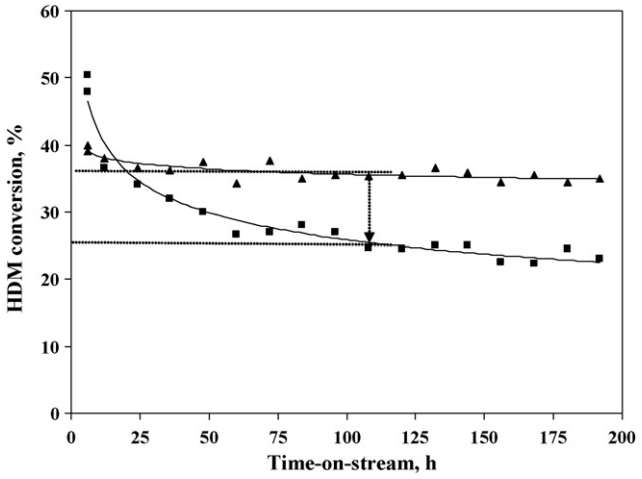

Fig. 5. Effect of support composition on the hydrodemetallization of Maya heavy crude: [(▲) NiMo/AS-31; (■) NiMo/AS-56].

silica content on support. Similar type of deactivation results for both catalysts observed for hydrodenitrogenation (HDN) as shown in Fig. 4. However, due to the role of acidic sites towards nitrogen molecular adsorption properties on catalytic sites, the HDN activity difference between the two catalysts is much lower compared with HDS. The HDN conversion of crude oil is relatively complicated due to presence of different kind of nitrogen organic-molecules (basic and non basic). The cleavage of C–N bond in a heterocyclic aromatic ring can only take place after ring hydrogenation, which is promoted by the presence of acidic sites. Moreover, pyrrol is a by-product of the metal porphyrin reaction (HDM), thus, the HDN conversion level also depends on HDM conversion.

The role of acidic sites can be also observed in the case of hydrodemetallization as shown in Fig. 5. It is also reported that the acid sites generated by the support may have some role to the HDM catalytic activity [27] but these acid sites are likely to deactivate with faster rate than those generated by metallic catalytic sites. Recently, Rana et al. [28] proposed a hydrodemetallization reaction mechanism in which HDM started on the Brønsted acid sites (–SH) through the adsorption of porphyrinic complex molecule. Thus, the HDM deactivation results are in agreement with the acid sites presence and that is most likely due to the nature or contribution of the support because the amount of supported phases (i.e. –SH group) is similar in both catalysts. Compared with HDS and HDN activities the HDM activity for both catalysts is less affected by the composition of the support. The variation in HDM and HDS can be due to the different pore diameter of the catalysts. Usually, HDM activity increases with increasing average pore diameter while HDS activity decreases [24]. When pore diameter is large the surface area becomes smaller, which makes very difficult to have high dispersion of active metals (NiMoS). In this regard, it is probable that either the catalyst should be bimodal or used for a particular application, such as HDS with high surface area or high dispersion, while HDM can be effectively achieved on the large pore diameter or low surface area catalyst [29].

Contrary to these results of HDS, HDN and even HDM, the hydrodeasphaltenization (HDAs) activity for these catalysts is relatively different as shown in Fig. 6. Although the deactivation with time-on-stream showed similar tendency, the presence of acid sites is clearly evident for asphaltene conversion. The higher acidity (high cumene cracking) containing catalyst has higher HDAs but lower HDS, HDN and HDM activity. This behavior can be explained in two ways that is either due to the pore diameter or due to the acidity. However, the combination of both properties favors the HDAs because the effectively diffusion of asphaltene

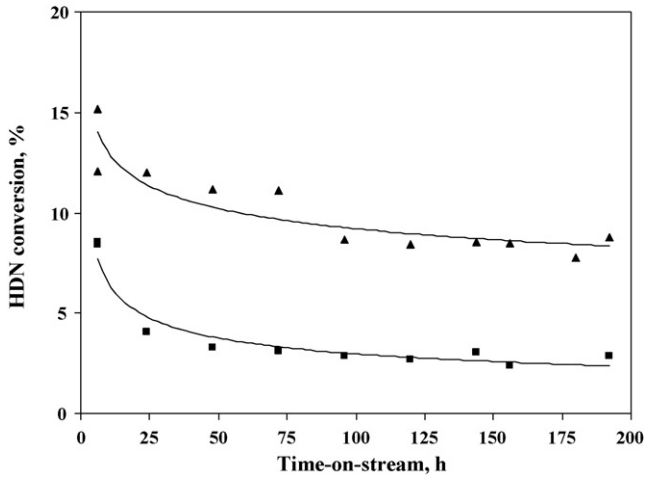

Fig. 4. Effect of support composition on the hydrodenitrogenation of Maya heavy crude: [(▲) NiMo/AS-31; (■) NiMo/AS-56].

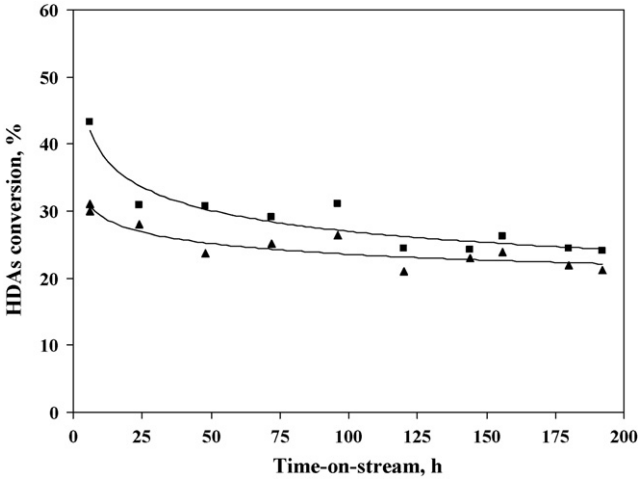

Fig. 6. Effect of support composition on the hydrodeasphaltenization of Maya heavy crude: [(▲) NiMo/AS-31; (■) NiMo/AS-56].

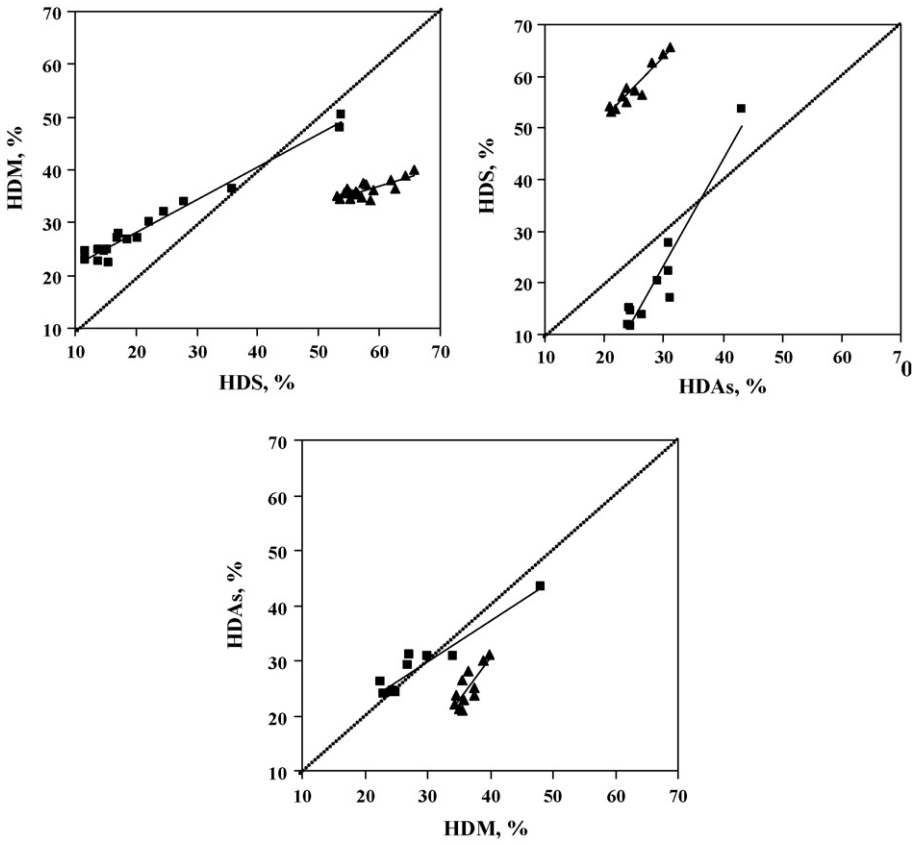

Fig. 7. Different selectivity of reaction products along with time-on-stream: [(▲) NiMo/AS-31; (■) NiMo/AS-56].

molecule occurs in large pore (macro-pores) and later enhances the cracking of molecule.

To elucidate about the effect of the different nature of catalytic sites, various selectivities are drawn in Fig. 7. These selectivity results indicated that the variation in activity is due to the combined effect of acidity as well as pore diameter of the catalyst. The HDM activity showed more or less similar tendency with HDAs, while HDS activity indicates entirely different results for the two catalysts. The explanation behind the selectivity towards HDM and HDAs is the nature and size of molecules and similar role of acidic sites for both activities. It appears from these results that the catalyst for heavy oil processing necessarily requires large pore diameter along with optimum dispersion of active metals, which are responsible for the catalytic reaction. However, the acidity of catalyst is a secondary parameter for catalyst design and will also depend on the selectivity of the desired product.

5. Characterization of spent catalysts

Fresh and spent catalysts were characterized by BET specific surface area, pore volume and pore size distribution and the results are presented in Table 5. The spent catalyst surface area and pore volume decrease by 40–50% for both catalysts. Spent catalyst

Table 5
Textural properties of fresh and spent catalysts

Property	NiMo/AS-31		NiMo/AS-56	
	Fresh	Spent	Fresh	Spent
SSA ($m^2\ g^{-1}$)	255.4	106	167.5	73.1
TPV ($cm^3\ g^{-1}$)	0.541	0.268	0.586	0.295
% Pore available				
Micro-pore	1.2	4.9	1.4	2.3
Meso-pore	93.5	89.8	73.9	65.2
Macro-pore	5.3	5.3	24.7	32.5
APD (nm)	8.5	10.1	14	16.1
% Volume (PSD)				
<5 nm	19.5	2.4	7.9	8.5
5–10 nm	31.1	2.9	15.7	11.4
10–25 nm	33.5	14.3	27.6	24.9
25–50 nm	10.5	32.1	24.7	22.8
50–100 nm	4.1	27.4	16.2	20.4
>100 nm	1.3	20.8	8.6	12.0

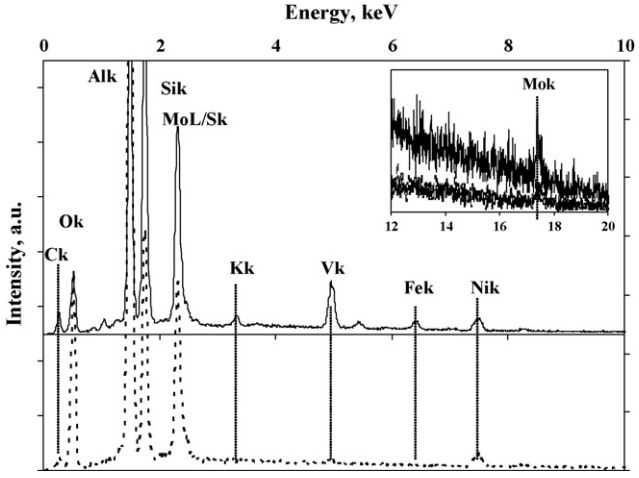

Fig. 8. EDX spectra of the spent catalysts deposited elements on the spent catalysts: [(- - - -) NiMo/AS-31; (–) NiMo/AS-56].

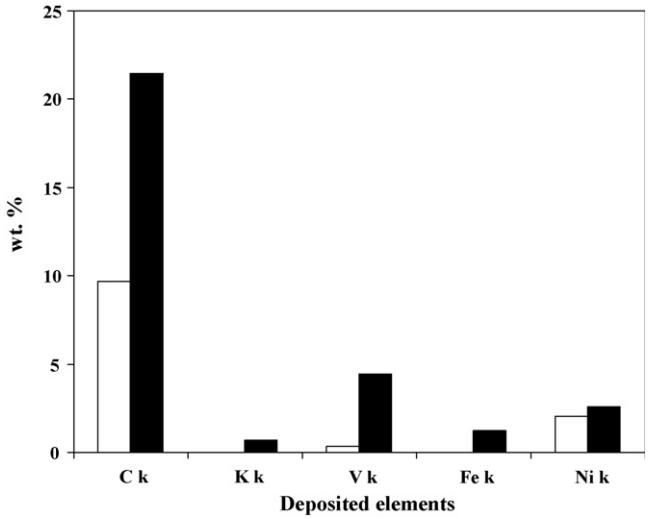

Fig. 9. Quantitative (average) analysis of deposited elements on spent catalysts: [(□) NiMo/AS-31; (■) NiMo/AS-56].

observed slight increase in micro-pore, which could be explained by substantial meso- and macro-pore blocking caused by the carbon and metal deposition during the reaction. This publication depicts the surface carbon and feed metals deposition on aged catalyst using SEM–EDX analysis. The selected point analysis of deposited species and spent catalyst composition is shown in Fig. 8. The large pore diameter catalyst possesses large amount of metal deposits as shown for NiMo/AS-56 catalyst. The quantitative values of deposited species are presented in Fig. 9. These facts of metal and carbon depositions are due to the effect of catalysts composition and their pore diameter and have a good correlation

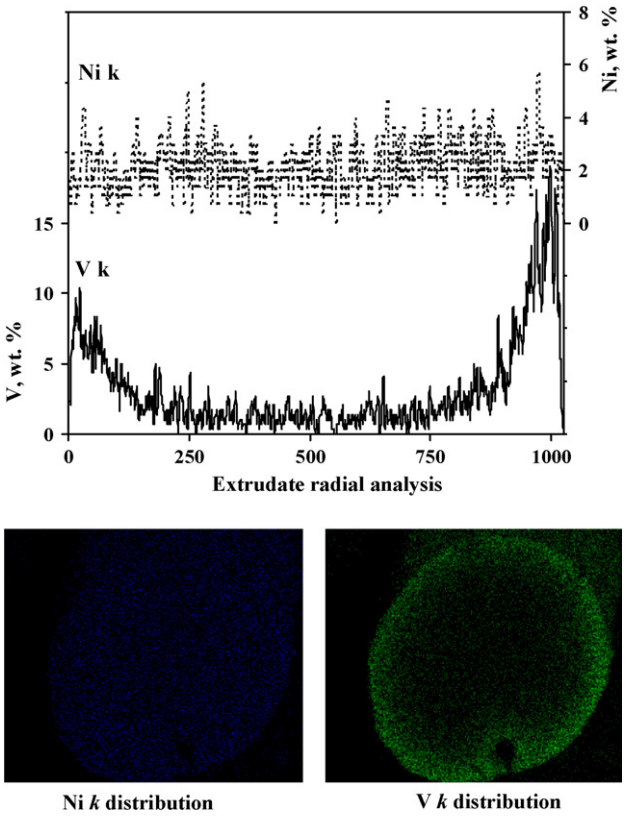

Fig. 10. SEM–EDX analysis of spent catalyst (NiMo/AS-31-S) Ni and V distributions.

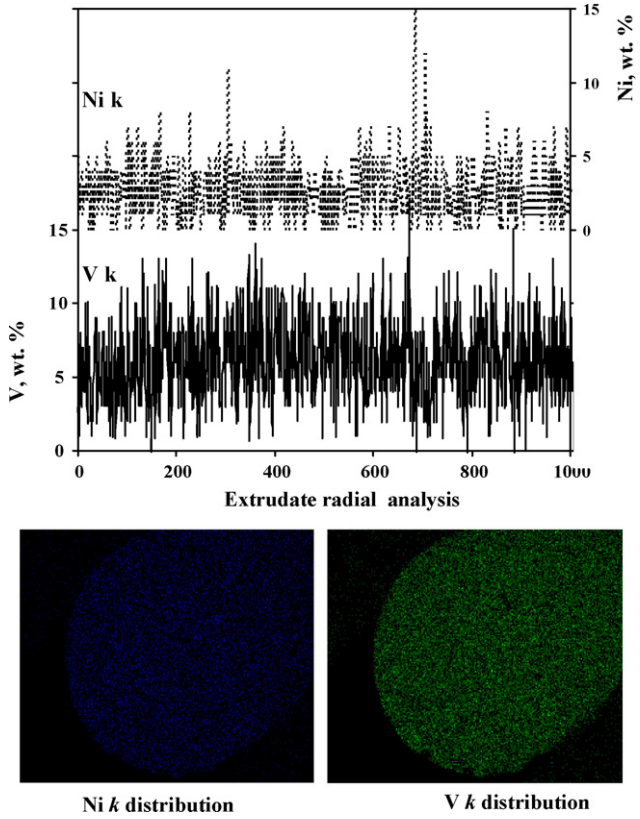

Fig. 11. SEM–EDX analysis of spent catalyst (NiMo/AS-56-S) Ni and V distributions.

with cumene cracking activity, which corresponds to the number of acid sites presented by the catalysts. To have a deeper insight of the catalyst deactivation linear analyses of extrudate and the deposition profiles for NiMo/AS-31 and NiMo/AS-56 were performed, whose results are shown in Figs. 10 and 11 respectively. The large pore catalyst has large amount of deposition along with extrudate while for the smaller pore diameter catalyst the metals are deposited more on the surface. Moreover, the Ni is relatively more distributed than vanadium which is deposited only on the outer surface of the catalyst. The results indicated that the diffusion of Ni complex molecule is better than vanadium one which could be due to its molecular size and/or intrinsically slower de-nickelation kinetic rate. It is also reported that the Ni complex molecule is more refractory than vanadium [30]. On the other hand the distribution profile for Ni and V is quite similar in the case of large pore diameter catalyst (Fig. 11). The aquired Ni and V mapping information sheds a new dimension for the study of deactivation of the outer and inner surface with respect to the different pore diameter of supported catalysts.

6. Conclusion

Large pore diameter Al_2O_3-SiO_2 acidic mixed oxide supports were prepared by using homogeneous co-precipitation method. NiMo supported catalysts hydroprocessing activities confirmed that deactivation at the initial period is due to carbon deposition, while progressive deactivation is due to the metal deposition on the surface of catalyst. The acidic properties of supported catalysts are crucial characterization on the way of catalyst deactivation, particularly for carbon deposition. The spent catalyst characterization results are concluding that the depositions of vanadium and nickel sulfides mainly depend on the diameter of the pores. As an effect of pore diameter, the larger pore diameter catalyst

contains higher amount of deposited species, which is distributed proportionally along with extrudate radius, while for smaller pore diameter catalyst the deposition mainly occurs on the extrudate surface.

References

[1] J. Ancheyta, M.S. Rana, E. Furimsky, Catal. Today 109 (2005) 1–2.
[2] J. Ancheyta, M.S. Rana, E. Furimsky, Catal. Today 109 (2005) 3–15.
[3] M.S. Rana, J. Ancheyta, P. Rayo, Catal. Today 109 (2005) 24–32.
[4] R. Tanaka, J.E. Hunt, R.E. Winans, P. Thiyagarajan, S. Sato, T. Takanohashi, Energy Fuels 17 (2003) 127–134.
[5] H. Seki, F. Kumata, Energy Fuels 14 (2000) 980–985.
[6] J.G. Speight, The Desulfurization of Heavy Oils and Residua, Marcel Dekker Inc., New York, 2000, p. 193.
[7] C. Leyva, M.S. Rana, F. Trejo, J. Ancheyta, Ind. Eng. Chem. Res. 46 (23) (2007) 7448–7466.
[8] P. Rahimi, T. Gentzis, E. Cotté, Energy Fuels 13 (1999) 694.
[9] G. Marroquín, J. Ancheyta, J.A.I. Díaz, Catal. Today 98 (2004) 75–81.
[10] P. Rayo, J. Ancheyta, J. Ramirez, A. Gutierez-Alejandre, Catal. Today 98 (2004) 171–179.
[11] M.S. Rana, J. Ancheyta, S.K. Maity, P. Rayo, Catal. Today 109 (2005) 61–68.
[12] S.K. Maity, J. Ancheyta, L. Soberanis, F. Alonso, Appl. Catal. A: Gen. 250 (2003) 231–238.
[13] C.J. Brinker, G.W. Scherer, Sol–Gel Science—The physics and Chemistry of Sol–Gel Processing, Academic Press, London, 1990.
[14] I. Jaymes, A. Douy, D. Massiot, J.-P. Busnel, J. Am. Ceram. Soc. 78 (10) (1995) 2648–2654.
[15] L.F. Nazar, L.C. Klein, J. Am. Ceram. Soc. 71 (1988), C-85-C-87.
[16] V. La Parola, G. Deganello, S. Scirè, A.M. Venezia, Solid State Chem. 174 (2003) 482.
[17] C. Leyva, M.S. Rana, J. Ancheyta, Catal. Today 130 (2008) 345–353.
[18] K. Tanabe, Solid Acids and Bases, Academic Press, New York, 1970.
[19] M.S. Rana, B.N. Srinivas, S.K. Maity, G. Murali Dhar, T.S. Prasada Rao, J. Catal. 195 (2000) 31–37.
[20] P. Ratnasamy, H. Knözinger, J. Catal. 54 (1978) 155–165.
[21] N.-Y. Topsøe, H. Topsøe, J. Catal. 139 (1993) 641–651.
[22] G. Muralidhar, F.E. Massoth, J. Shabtai, J. Catal. 85 (1984) 44–52.
[23] S. Sivasanker, A.V. Ramaswamy, P. Ratnasamy, in: H.F. Barry, P.C.H. Mitchell (Eds.), Proceedings, 3rd International Conference on Chemistry & Uses of Molybdenum, Climax Molybdenum Co., Ann Arbor, MI, 1979, p. 98.
[24] M.S. Rana, J. Ancheyta, P. Rayo, S.K. Maity, Catal. Today 98 (2004) 151–160.
[25] M.S. Rana, J. Ancheyta, S.K. Maity, P. Rayo, Petrol. Sci. Technol. 25 (2007) 187–213.
[26] M.S. Rana, J. Ancheyta, S.K. Maity, P. Rayo, Catal. Today 104 (2005) 86–93.
[27] P. Rayo, J. Ramírez, J. Ancheyta, M.S. Rana, Petr. Sci. Tech. 25 (2007) 215–229.
[28] M.S. Rana, J. Ancheyta, P. Rayo, S.K. Maity, Fuel 86 (9) (2007) 1263–1269.
[29] S. Eijsbouts, Stud. Surf. Sci. Catal. 127 (1999) 21.
[30] M.S. Rana, S.K. Maity, J. Ancheyta, Maya heavy crude oil hydroprocessing catalysts, in: James G. Speight, Jorge Ancheyta (Eds.), Hydroprocessing Heavy Oil and Residua, Taylor & Francis-Taylor & Francis, New York, 2007, , Chapter 7.